https://doi.org/10.5194/egusphere-2024-2233
Preprint. Discussion started: 29 July 2024
© Author(s) 2024. CC BY 4.0 License.

In situ Cosmogenic ^{10}Be and ^{26}Al in Deglacial Sediment Reveals Interglacial Exposure, Burial, and Limited Erosion Under the Quebec-Labrador Ice Dome

Peyton M. Cavnar[1,2], Paul R. Bierman[1,2], Jeremy D. Shakun[3], Lee B. Corbett[1], Danielle LeBlanc[3], Gillian L. Galford[1,2], and Marc Caffee[4]

[1]Rubenstein School for the Environment and Natural Resources, University of Vermont, Burlington, 05405, United States

[2]Gund Institute for the Environment, Burlington, 05405, United States

[3]Department of Earth and Environmental Sciences, Boston College, Chestnut Hill, 02467, United States

[4]PRIME Laboratory, Purdue University, West Lafayette, 47907, United States

Correspondence to: Peyton M. Cavnar (cavnar.peyton@gmail.com)

Abstract. To understand the erosivity of the eastern portion of the Laurentide Ice Sheet and the isotopic characteristics of the sediment it transported, we sampled buried sand from deglacial features (eskers and deltas) across eastern Canada (n=10), a landscape repeatedly covered by the Quebec-Labrador Ice Dome. We measured concentrations of ^{10}Be and ^{26}Al in quartz isolated from the sediment and, correcting for sub-surface cosmic-ray exposure after Holocene deglaciation, used these results to determine nuclide concentrations at the time the ice sheet deposited the sediment. To determine what percentage of sediment moving through streams and rivers currently draining the field area was derived from incision of thick glacial deposits as opposed to surface erosion, we used ^{10}Be and ^{26}Al as tracers by collecting and analyzing modern river sand sourced from Holocene-exposed landscapes (n=11).

We find that all ten deglacial sediment samples contain measurable concentrations of ^{10}Be and ^{26}Al equivalent on average to several thousand years of surface exposure—after correction, based on sampling depth, for post-deposition Holocene nuclide production. Error-weighted averages (1 standard deviation errors) of measured $^{26}Al/^{10}Be$ ratios for both corrected deglacial (6.1±1.2) and modern sediment samples (6.6±0.5) are slightly lower than the production ratio at high latitudes (7.3±0.3) implying burial and preferential decay of ^{26}Al, the shorter-lived nuclide. However, five deglacial samples collected closer to the center of the former Quebec-Labrador Ice Dome have much lower corrected $^{26}Al/^{10}Be$ ratios (5.2±0.8) than five samples collected closer to the former ice margins (7.0±0.7). Modern river sand contains on average about 1.75 times the concentration of both nuclides than deglacial sediment corrected for Holocene exposure.

The ubiquitous presence of ^{10}Be and ^{26}Al in eastern Quebec deglacial sediment is consistent with many older-than-expected exposure ages, reported here and by others, for bedrock outcrops and boulders once covered by the Quebec-Labrador Ice Dome. Together, these data suggest that glacial erosion and sediment transport in eastern Canada were insufficient to remove material containing cosmogenic nuclides produced during prior interglacial periods both from at least some bedrock outcrops and from all glacially transported sediment we sampled. Near the center of the Quebec-Labrador Ice Dome, ratios of $^{26}Al/^{10}Be$ are consistently below those characteristic of surface production at high latitude. This suggests burial of the glacially transported sediment for at least many hundreds of

https://doi.org/10.5194/egusphere-2024-2233
Preprint. Discussion started: 29 July 2024
© Author(s) 2024. CC BY 4.0 License.

thousands of years and thus the possibility that ice at the center of the Quebec-Labrador Ice Dome survived many interglacials when more distal ice melted away.

1. Introduction

Ice sheets are important geomorphic agents of high-latitude landscape change, and their activity reflects changes of climate on a global scale. During the Last Glacial Maximum (LGM), about 20-25 ka, the Laurentide Ice Sheet (LIS) was the largest body of ice in the Northern Hemisphere, covering most of Canada and the northern United States (Dalton et al., 2022). Its disappearance during the latest Pleistocene and early Holocene (characterized by collapse of northern Canadian ice domes) revealed a complicated paraglacial landscape: one in which cycles of advance and retreat left behind deglacial landforms (both bedrock and sedimentary) while overriding, altering, and eroding those created previously (Occhietti et al., 2011). Because of this, in most places it is difficult to ascertain from the landscape much about LIS behavior prior to the LGM although landscape analysis in far northern Canada suggests inheritance of some bedrock landscape features from prior times of glaciation (Rice et al., 2020).

Understanding paleo ice sheet behavior is important because it indicates how and when prior ice sheets melted during warming periods and readvanced when the climate cooled. Sub-glacial erosion not only shapes landscapes, but it also generates sediment that is both deposited on land and in adjacent marine basins. Such glacially derived marine sediment records millions of years of ice history and when cored can be used to understand past climates and ice sheet response (e.g., Larsen et al., 1994). More recently, analyses of cosmogenic nuclides in marine sediment have been used to decipher the Pleistocene history of the Greenland Ice Sheet (Bierman et al., 2016) and to suggest that the LIS did not completely melt away during some and perhaps many interglacials of the last million years (LeBlanc et al., 2023).

In this paper, we use cosmogenic nuclide concentrations to study glacially derived sediment deposited beneath and adjacent to the now-vanished LIS. We present concentrations of ^{10}Be and ^{26}Al measured in quartz isolated from buried deglacial sediments and modern river sand in Labrador and Quebec, Canada. After correcting isotopic concentrations of deglacial sediment for Holocene nuclide production, we use these data and ^{26}Al/^{10}Be ratios to infer paleo ice sheet persistence, erosion, and sediment transport efficiency, as well as to constrain the source of sediment in modern rivers. These results allow us to infer LIS behavior and erosivity during the late Pleistocene and improve interpretation of cosmogenic analysis of glacially-derived sediment in marine sediment cores such as those of LeBlanc et al. (2023).

2. Background

We know little about the LIS's erosion and sediment transport behavior prior to the LGM because, each time the ice sheet advanced, it overran and remobilized datable sedimentary and morphological evidence of previous glaciations such as moraines, eskers, and ice-contact deltas. Because of this, few terrestrial records remain of pre-LGM LIS behavior. In Quebec and Labrador, abundant streamlined bedrock outcrops, scoured lake basins, and multiple sets of striations provide evidence for a once-erosive LIS with warm-based, fast-sliding ice (Kleman et al., 1994; Roy et al., 2009; Dalton et al., 2019). However, models commonly suggest that this region featured some of

https://doi.org/10.5194/egusphere-2024-2233
Preprint. Discussion started: 29 July 2024
© Author(s) 2024. CC BY 4.0 License.

the most cold-based and slowest moving ice of the entire LIS during the last glaciation (Tarasov and Peltier, 2007; Stokes et al., 2012; Melanson et al., 2013). Because the advancing LIS destroyed evidence of its past deposits and ice margin positions, it is difficult to disentangle the timing of cross-cutting striation formation (Kleman et al., 2010); thus, our knowledge about how erosive or extensive this sector of the LIS was prior to the LGM is limited (Dalton et al., 2019; Batchelor et al., 2019).

2.1. Using Cosmogenic Nuclides to Study Complex Glacial and Post-Glacial Histories

Cosmogenic nuclides provide a means to understand paleo ice sheet behavior. These nuclides are rare isotopes, such as ^{10}Be and ^{26}Al, created when cosmic radiation bombards minerals at and near Earth's surface including weathering-resistant quartz (Gosse & Phillips, 2001). Most nuclide production occurs within several meters of the surface via spallation reactions between neutrons and target elements in rock. A small amount of nuclide production is caused by smaller particles, muons, but because muons have low reactivity with matter, they can penetrate far more deeply below the surface than neutrons (Braucher et al., 2011). At depths below several meters, muons are responsible for most subsurface production of cosmogenic nuclides (Braucher et al., 2003).

Because ^{10}Be and ^{26}Al are created in both rock and glacially deposited sediment, we can analyze their concentrations to infer the depth of glacial erosion, the persistence of glacial sediment on the landscape, and set limits on the extent and timing of sediment and rock burial by ice sheets (e.g., Briner et al., 2016; Bierman et al., 2016; Marsella et al., 2000; Corbett et al., 2016b; Stroeven et al., 2002; Staiger et al., 2006; Harbor et al., 2006). The half-lives of ^{10}Be and ^{26}Al differ by a factor of two (~1.36 and ~0.73 My, respectively) and hence they decay at different rates. This dual isotope approach allows for a more detailed understanding of glacial presence over time (burial during which time nuclide production ceases) and the persistence of surficial materials (exposure when nuclide production occurs) (e.g., Nishiizumi et al., 2007; Nishiizumi, 2004; Nishiizumi et al., 1991; Bierman et al., 1999).

In situ ratios of ^{26}Al/^{10}Be at production are 7.3 ±0.3 (1σ) in high-latitude regions (Corbett et al., 2017). When a landscape is covered by a thick layer of ice such as the LIS, or if sediment is stored in deposits deep enough to prevent most cosmic ray penetration, production of *in situ* ^{26}Al and ^{10}Be slows or stops. As isotopes produced during initial exposure decay, the ^{26}Al/^{10}Be ratio falls (Klein et al., 1986; Bierman et al., 1999; Balco et al., 2005). This change becomes reliably measurable only after several hundred thousand years of burial. Re-exposure to cosmic rays at or near Earth's surface will raise the ^{26}Al/^{10}Be ratio back toward that at production. However, if sediment is buried meters below the surface during interglacial periods (such as in deglacial deltas, coastal bluffs, or eskers), ^{26}Al/^{10}Be ratios depressed by LIS ice cover and/or storage in sedimentary deposits can be preserved (Corbett et al., 2016b; Bierman et al., 2016; Balco et al., 2005). Conversely, sediment, if it is sourced close to the surface, will have a higher ^{26}Al/^{10}Be ratio because of recent exposure to cosmic radiation (Nelson et al., 2014).

Concentrations of ^{10}Be and ^{26}Al in glacial sediment reflect the history of that sediment and of the ice sheet that produced it over time. Long interglacial exposures, thin sediment cover, and bedrock that is resistant to erosion will allow high concentrations of nuclides to accumulate – for example, in central North America (Balco et al., 2005). Persistent ice cover, high rates and depths of glacial erosion, and efficient sediment transport by ice will

https://doi.org/10.5194/egusphere-2024-2233
Preprint. Discussion started: 29 July 2024
© Author(s) 2024. CC BY 4.0 License.

lower nuclide concentrations in glacially derived sediment, such as in southern and western Greenland (Nelson et al., 2014).

2.2. Laurentide Ice Sheet History and Deglaciation in Eastern Canada

For most of its recent inception (~118 ka) to final deglaciation (~8 ka), the LIS was characterized by three major ice domes, regions of especially thick, outflowing ice (~4 km in some places): Foxe Baffin Dome, Keewatin Dome, and the Quebec-Labrador Dome (Stokes et al., 2012; Dalton et al., 2022). Modeling suggests the formation of the Foxe Baffin Dome first (~118 ka), with ice growth then progressing southward to create the Keewatin Dome (~116 ka), and later the nucleus of the Quebec-Labrador Ice Dome (~114 ka) (Stokes et al., 2012). These domes coalesced into a single ice body and separated again as the LIS waxed and waned during its overall buildup through the last glacial cycle (Stokes et al., 2012; Dalton et al., 2022).

Changes in LIS size are thought to have tracked the global marine oxygen isotope record, though uncertainties in ice volume and extent through time reflect the paucity of geologic constraints. For instance, the majority of Canada may have been ice-covered with the LIS reaching 70% of its LGM extent as early as Marine Oxygen Isotope (MIS) stage 5d (~110 ka) or not until MIS 4 (~60 ka) (Dalton et al., 2022). In contrast, the deglacial retreat of the LIS in eastern Quebec following the LGM is well constrained (Dalton et al., 2022; Ullman et al., 2016; Couette et al., 2023) (Figure 1).

It is debated how extensive and persistent the LIS was during Pleistocene interglacials (Zhou and McManus, 2023; LeBlanc et al. 2023). Cosmogenic nuclides in ice-rafted debris (IRD) from LIS icebergs discharged during the last glacial period have been used to infer the burial and exposure history of glacial sediment prior to its transport to the ocean (LeBlanc et al., 2023). These IRD ^{26}Al/^{10}Be ratios averaged 4.7±0.8 (LeBlanc et al., 2023), which is much lower than the high latitude production value of 7.3±0.3 (Corbett et al., 2017). Such depressed ratios require long (>million year) periods of burial (presumably by ice) throughout the Pleistocene, as interglacials with little to no ice would have yielded IRD with higher ratios from near-surface exposure (LeBlanc et al., 2023). LeBlanc et al.'s cosmogenic data challenge the commonly held assumption that all Pleistocene interglacials resulted in fully ice-free conditions in eastern Canada for at least thousands of years.

A similar debate concerns the magnitude of LIS retreat during interstadials within the last glacial period. A combination of luminescence dating, ^{14}C dating, and cosmogenic nuclides (^{10}Be and ^{26}Al), along with evidence of a marine incursion into Hudson Bay, suggest that the portion of the LIS over Hudson Bay deglaciated during MIS 3 (Dalton et al., 2019; Miller and Andrews, 2019). However, the reliability of these ages has been questioned and the timing of carbonate-rich Heinrich events H5 and H4 suggest that an intact Hudson Strait ice stream existed during MIS 3 (Miller & Andrews, 2019). With this debate unsettled, it remains uncertain how much the LIS ice margin retreated during interstadial periods.

Other studies have investigated LIS sensitivity to climate shifts on even finer time scales during the last deglaciation. For instance, there is evidence for ties between regional deglaciation and climate fluctuations based on 37 ^{10}Be exposure ages in eastern Quebec and Labrador (Couette et al., 2023). These data are interpreted as indicating five still-stands or re-advances of the eastern LIS margin (~12.9 ka, ~11.5 ka, ~10.4 ka, ~9.3 ka, and

https://doi.org/10.5194/egusphere-2024-2233
Preprint. Discussion started: 29 July 2024
© Author(s) 2024. CC BY 4.0 License.

~8.4-8.2 ka) before its final collapse (Couette et al., 2023). These periods correspond with abrupt cooling events recorded in Greenland ice cores, likely triggered by meltwater discharge from the LIS (Couette et al., 2023). These recurring cold episodes may have helped delay final deglaciation of the Quebec-Labrador Ice Dome until ~4 ka after peak Holocene insolation and CO_2 forcing (Ullman et al., 2016), making it a part of the LIS that lasted longer than most after the LGM (Dalton et al., 2020).

2.3. Cosmogenic Nuclides as Tracers of Sediment Sourcing

Cosmogenic nuclides have been used to identify sediment sources for both modern and paleo ice sheets. For example, Nelson et al., (2014) sampled rivers in the deglaciated areas of coastal Greenland. They found that ^{10}Be concentrations in Greenland sediment sourced from the ice sheet (6,500 ± 4,100 atoms g^{-1}) were significantly lower than sediment sourced from deglaciated terrain (14,900 ± 8,600 atoms g^{-1}, Nelson et al., 2014). This difference can be explained by contrasting exposure histories. Outboard of the ice margin ^{10}Be concentrations in sediment increased when exposed to cosmic radiation since Holocene deglaciation while concentrations remained low under the ice sheet where production of ^{10}Be is minimal. Sediments sourced from a mix of deglaciated and glaciated areas have ^{10}Be concentrations that are much closer to those of the glacial than deglacial terrains. These results therefore suggest most sediment moving through river systems in glacial and paraglacial landscapes in Greenland comes from under the glacier as opposed to the adjacent deglaciated areas.

In southwest Minnesota and eastern South Dakota, a similar approach was used to determine sediment sourcing in a deglaciated part of the midwestern United States (Balco et al., 2005). They inferred that modern river sediments were sourced primarily from rapid erosion of riverbanks that exposed glacial deposits because of similar ^{10}Be and ^{26}Al concentrations (~60,000 and 270,000 atoms g^{-1}, respectively) and much lower than production ^{26}Al/^{10}Be in both (4.70 ± 0.29; n=9). If the modern sediment had come from slowly-eroding surfaces exposed to cosmic radiation after deglaciation, it would have had nuclide concentrations higher than deglacial sediment and higher ^{26}Al/^{10}Be.

2.4. Assessing the Erosivity of Ice Sheets

Previously-published ^{10}Be concentrations in bedrock and boulders within the historical range of the Quebec-Labrador Ice Dome reveal a varied pattern of erosion. Some areas were deeply eroded while others show evidence for inherited ^{10}Be and less effective subglacial erosion (Ullman et al., 2016; Couette et al., 2023). For example, of the five boulders sampled by Couette et al. (2023) from the early Holocene Paradise Moraine in eastern Labrador, two have significant and obvious inheritance of nuclides from prior exposure with ^{10}Be ages >20 ka, while the remaining three inaccurately date the moraine as older than a margin further from the center of the ice dome. Ullman et al. (2016) likewise found anomalously high ^{10}Be concentrations in 10 out of 65 boulders along transects stretching eastward and southward from the center of the Quebec-Labrador Dome to the coast.

Comparable results have been found near the margin of other ice sheets. In western Norway, glacial erratic boulders on the island of Utsira, near the former margin of the Scandinavian Ice Sheet, have ^{10}Be ages that are >10% too old (~20 ka) based on independent radiocarbon constraints on the timing of deglaciation (Briner et al., 2016).

https://doi.org/10.5194/egusphere-2024-2233
Preprint. Discussion started: 29 July 2024
© Author(s) 2024. CC BY 4.0 License.

The uniform concentration of inherited ^{10}Be among all samples suggests that the elevated nuclide concentrations are the product of muon-induced production at depth rather than surface exposure where the sides and the bottom of boulders would have different concentrations than the top (Briner et al., 2016). Assuming brief ice cover only during maximum glacial phases, long interglacial exposure times at Utsira coupled with ineffective glacial erosion helped create and preserve this inherited muon-produced ^{10}Be.

Along Greenland's western ice margin, most subglacial cobbles (72 out of 86) sampled had an extremely low concentration of ^{10}Be (median = 1.0 x 10^3 atoms g^{-1}), indicative of deep subglacial erosion and/or minimal prior surface exposure (Corbett et al., 2021). But, a subset of samples had higher ^{10}Be concentrations (> 3 x 10^3 atoms g^{-1}, n = 14), suggesting sourcing from minimally erosive, cold-based regions where bedrock and sediment still contained ^{10}Be accumulated during prior ice-free periods (Corbett et al., 2021). Halsted et al. (2023) and Colgan et al. (2002) found similar inheritance of ^{10}Be in boulders and bedrock sampled near the former LGM margin of the LIS and attributed higher than expected concentrations of ^{10}Be to minimal erosion during the brief time the ice occupied the marginal position.

3. Study Site

The Quebec-Labrador Ice Dome occupied the eastern subarctic Canadian Shield, where bedrock consists of mostly Proterozoic quartzofeldspathic gneisses and granites (Hynes & Rivers, 2010). Soils are thin and punctuated by prominent bedrock outcrops and large glacial erratics (Ullman et al., 2016). Central and southern Quebec-Labrador also includes multiple moraine systems that track the final deglaciation of the ice dome into the early Holocene (Ullman et al. 2016). There are eskers and substantial ice contact deltas where the ice front during deglaciation met a body of standing water (Liverman, 1997; Storrar et al., 2013). The paraglacial landscape is still experiencing isostatic glacial rebound, with greater changes in elevation since deglaciation towards the former dome center (Andrews & Tyler, 1977). Prominent isostatic rebound has occurred near James Bay and southern Hudson Bay, with ~300 m of rebound compared to ~100 m along coastal eastern Labrador (Andrews & Tyler, 1977).

Notable geographic features of this region include the St. Lawrence River, the Churchill River, and the Manicouagan Reservoir, an annular lake north of the Gulf of St. Lawrence formed in a depression caused by a meteor impact (Spray et al., 1998). The St. Lawrence River flows from southwest to northeast and is located southeast of the Quebec-Labrador Ice Dome's center (Süfke et al., 2022). During final LIS deglaciation, the St. Lawrence River served as one of the major meltwater drainage systems (Süfke et al., 2022). The Churchill River flows east from the former center of the Quebec-Labrador Dome, draining into Lake Melville and then the Atlantic Ocean (Canadian Geographic, n.d.).

Eastern Canada is dominated by boreal spruce forests, sedges, and muskegs (shallow bogs covered in moss) (Payette et al., 1989). This sub-arctic ecosystem is prone to burning during arid periods in the summer, with a recorded fire history stretching back to the 1950's (Payette et al., 1989). Northern Quebec and Labrador are classified under the Dfc climate zone (cool continental climate/subarctic) according to the Koppen climate classification system (Amani et al., 2019; Beck et al., 2018). During winter, ground-based measurements record a mean of ~158 millimeters (mm) of snow water equivalent (SWE) for eastern Canadian boreal forests (Larue et al., 2017).

4. Methods & Materials

4.1. Study Design

Our primary goal is to measure and understand the concentrations of cosmogenic nuclides in sediment moved by the LIS in eastern Canada along a 1000-km transect (Figure 1). To constrain nuclide concentrations in materials deposited by the LIS (Table 1), we sampled deglacial sediment deposits (n=10) including ice-contact deltas and eskers as well as contemporary river sediment (Figure 2). We also collected modern river sediment samples (n=11) from main river trunks (St. Lawrence and Churchill River) as well as smaller tributaries to compare their ^{10}Be and ^{26}Al concentrations and $^{26}Al/^{10}Be$ ratios to those of deglacial samples to determine the source of sediment moving through contemporary streams and rivers (Table 1). We collected one sample from a bedrock outcrop. Our data provide context for measurements made in sand-sized sediment of glacial and interglacial age present in marine sediment cores collected offshore (LeBlanc et al. 2023).

4.2. Field Methods

We collected samples along a transect running westward from Goose Bay, Labrador through the former center of the Quebec-Labrador Ice Dome at Labrador City and then southward to the St. Lawrence River near Quebec City (Figure 1). We collected sediment from deltas and eskers on clean faces in gravel pits or along river bluffs from 2 to 30 meters (m) below the upper surface to reduce the effect nuclide production following deglaciation. We used shovels to dig ~0.3 m into the side of the landform before collecting ~500 g of sand. We collected one exposed bedrock sample (Table 1). Modern river sediment samples were collected along shorelines upstream of any nearby development.

Table 1. Sample Location and Type

Sample Name	Type [a]	Latitude [b] (°N)	Longitude [b] (°W)	Sample Site Elevation [b] (m)
CF-02	Deglacial Sediment	53.5077	-63.9545	167
LC-02	Deglacial Sediment	52.2011	-67.8722	537
LC-04	Deglacial Sediment	51.7102	-68.0719	440
LC-05	Deglacial Sediment	51.4881	-68.2192	391
MC-01	Deglacial Sediment	50.4748	-68.8101	500

https://doi.org/10.5194/egusphere-2024-2233
Preprint. Discussion started: 29 July 2024
© Author(s) 2024. CC BY 4.0 License.

MC-02	Deglacial Sediment	48.6452	-69.0854	10
GB-03	Deglacial Sediment	53.2572	-60.7848	36
GB-05	Deglacial Sediment	53.0922	-61.8920	402
SS-01	Deglacial Sediment	48.1030	-69.7213	10
SS-05	Deglacial Sediment	47.1669	-70.8047	307
CF-01	Modern River Sediment	53.5060	-63.9585	126
CF-05	Modern River Sediment	53.0595	-66.2555	527
LC-01	Modern River Sediment	52.3365	-67.5671	533
LC-03	Modern River Sediment	52.1107	-68.0073	645
LC-06	Modern River Sediment	51.4882	-68.2229	401
GB-02	Modern River Sediment	53.3934	-60.4229	2
GB-04	Modern River Sediment	53.2201	-60.9549	210
MC-03	Modern River Sediment	48.6779	-69.3045	61
SS-02	Modern River Sediment	47.8942	-69.9368	128
SS-03	Modern River Sediment	47.6665	-70.1589	3
SS-04	Modern River Sediment	47.5157	-70.5066	25
GB-06	Bedrock	53.3351	-62.9912	484

[a] Deglacial sediment is sand deposited from the LIS as it was retreating. Modern river sediment was collected from rivers and streams.

[b] Location and elevation were measured in the field using a Garmin eTrex 20 GPS

https://doi.org/10.5194/egusphere-2024-2233
Preprint. Discussion started: 29 July 2024
© Author(s) 2024. CC BY 4.0 License.

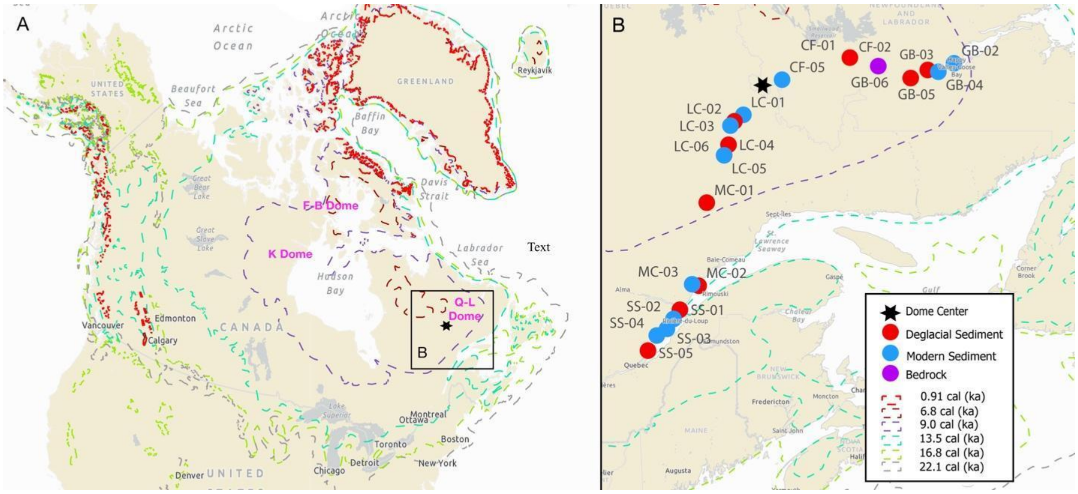

Figure 1. Map of field area. A. Overview of North America with field area demarcated by black outline. B. Sampling locations are color coded by type and with sample ID. The black star represents the center of the Quebec-Labrador Ice Dome, estimated to be close to modern day Labrador City (Ullman et al., 2016). Dotted lines represent LIS margins provided by Dalton et al. (2020). Different colored lines each correspond to a retreat isochron with calibrated radiocarbon age in ka (see legend).

https://doi.org/10.5194/egusphere-2024-2233
Preprint. Discussion started: 29 July 2024
© Author(s) 2024. CC BY 4.0 License.

Figure 2. Photographs of representative field sites**.** A. Modern river sediment at MC-03. B. Deglacial sediment at SS-05. C. Bedrock outcrop at GB-06. D. Deglacial sediment at MC-01.

4.3 Laboratory Methods

To isolate and purify quartz for cosmogenic nuclide analysis, we used a series of physical and chemical processes (Kohl & Nishiizumi, 1992). We sieved material to between 250 and 850 µm for further processing. For each sample, we performed two 24-hour 6 N hydrochloric acid etches in heated ultrasonic baths to remove grain coatings. We then used dilute (1%) hydrofluoric and nitric acid etches for three 24-hour periods after which we sonicated samples in 0.5% HF and HNO_3 for a minimum of two weeks (Kohl & Nishiizumi, 1992). We evaluated the purity of etched samples using inductively coupled plasma spectrometry optical emission (ICP-OES) after which impure samples were re-etched until they were sufficiently pure.

We extracted beryllium and aluminum from the purified quartz samples (17.3 –22.2 g, n =22) in the National Science Foundation/ University of Vermont Community Cosmogenic Facility using methods described in Corbett et al. (2016). Samples were prepared in two separate batches, each of which included a fully processed blank. We spiked the samples with ~250 µg ^{9}Be using a beryl carrier made in the Community Cosmogenic Facility with a Be concentration of 348 µg mL^{-1} (Table 4a). We spiked samples with SPEX ICP Al standard (1000 ppm) as needed based on their quantity of native Al, ensuring at least 1500 µg of total Al in every sample.

https://doi.org/10.5194/egusphere-2024-2233
Preprint. Discussion started: 29 July 2024
© Author(s) 2024. CC BY 4.0 License.

We quantified total Al in the samples by ICP-OES immediately following sample digestion. Following standard procedures (Corbett et al., 2016), we removed replicate aliquots from the samples by mass (representing ~2% and ~4% of the sample, respectively), added 25 µL H_2SO_4 to each, evaporated the HF, then diluted the residual H_2SO_4 droplets by mass with a 0.25% H_2SO_4 solution spiked with Y as an internal standard. Purdue Rare Isotope Measurement Laboratory performed accelerator mass spectrometry analysis. For $^{10}Be/^{9}Be$, measured ratios were normalized to primary standard 07KNSTD3110 with a ratio of 2850 x 10^{-15} (Nishiizumi et al., 2007). For $^{26}Al/^{27}Al$, analyses were normalized to primary standard KNSTD with a ratio of 1.818 x 10^{-12} (Nishiizumi et al., 2004).

4.4. Data Reduction

We used the known concentration of ^{9}Be added as carrier, along with the measured isotopic ratio and quartz mass to calculate the concentration of ^{10}Be in each sample. Because of the native ^{27}Al within the samples, the concentration of ^{27}Al measured using ICP-OES after quartz dissolution was used to calculate the concentration of ^{26}Al. We subtracted the mean extraction process blank ratios of $^{10}Be/^{9}Be$ ((7.41 ± 2.81) x 10^{-16}; n = 2) and $^{26}Al/^{27}Al$ ((5.39 ± 0.71) x 10^{-16}; n = 2) from the measured ratios and propagated the uncertainty in quadrature (Table 2). We used a 2-standard deviation (SD) threshold for detectability; that is, if twice the analytical uncertainty exceeded the measured ratio, then we considered the sample to be below detection limits. This provides a 95% confidence that the isotopic ratios and concentrations we report are finite. We use the same value (alpha = 0.05) for all statistical tests we perform. We used both Wilcoxon rank-sum tests (due to the non-normal distribution of nuclide concentrations in modern sediment samples) and Tukey HSD tests to investigate significant differences between sample groups.

Table 2. Measured Blank Isotope Ratio

Name	Batch Number	Al Cathode Number	Be Cathode Number	AMS $^{10}Be/^{9}Be$ Ratio	AMS $^{10}Be/^{9}Be$ Uncertainty	AMS $^{26}Al/^{27}Al$ Ratio	AMS $^{26}Al/^{27}Al$ Uncertainty
BLK	745	169457	169433	5.42 x 10^{-16}	2.71 x 10^{-16}	4.89 x 10^{-16}	7.04 x 10^{-16}
BLK	746	169470	169446	9.39 x 10^{-16}	5.77 x 10^{-16}	5.89 x 10^{-16}	8.49 x 10^{-16}

Both ^{26}Al blanks had 1 rare isotope count accounting for the large uncertainty.

4.5. Holocene Exposure Correction

For deglacial samples, we calculated the concentration of nuclides attributable to Holocene exposure. To do this, we used the online exposure age calculator formerly known as CRONUS (constant production rate model, version 3.0.2, constants 2020-08-26) to determine the surface production rate (atoms g^{-1} yr^{-1}) of ^{10}Be and ^{26}Al for both muons (P_{μ}) and spallation (P_s) at each sample site (Balco et al., 2008). The production rate at depth was then estimated using an attenuation length of 165 g cm^{-2} for spallation (Λ_s) and 1400 g cm^{-2} for muons (Λ_{μ}). We assumed a sediment density (ρ) of 1.7 g/cm^3. This allowed us to calculate the production of ^{10}Be and ^{26}Al (H in atoms g^{-1}) at each sampling depth (D in cm) since deglaciation (A in yr) taking deglaciation age estimates for each sample site from Ullman et al.(2016) and Dalton et al.(2020) and using equation 1.

https://doi.org/10.5194/egusphere-2024-2233
Preprint. Discussion started: 29 July 2024
© Author(s) 2024. CC BY 4.0 License.

$$H = P_s \cdot 1/exp\,(\frac{D \cdot \rho}{\Lambda_s}) \cdot A + P_\mu \cdot 1/exp\,(\frac{D \cdot \rho}{\Lambda_\mu}) \cdot A \qquad (1)$$

We checked how appropriate our apparent muonogenic attenuation factor was using the CRONUS implementation of Heisinger et al. (2002) (code P_mu_total.m) for sea level— yielding < 1% difference from our original calculations. We estimated 1σ uncertainties in the concentration of nuclides produced during the Holocene due to uncertainties in our sample depths (we use half our quoted uncertainty, which we consider a 95% confidence interval), and combined these in quadrature with measurement uncertainties (Table 3). To correct for Holocene exposure in our bedrock sample (GB-06), we multiplied the deglaciation age in this area (7.6 ka, from Ullman et al.'s CL3 transect) by the CRONUS-derived production rate at this site to estimate the concentration of nuclides produced following deglaciation. This concentration was subtracted from the sample's ^{10}Be concentration to calculate the concentration of inherited nuclides.

Table 3. Calculations for Holocene Exposure-Corrected Concentrations

Sample Name	Deglaciation Age (yr)	Sample Depth (cm)	Depth Uncertainty (cm)	^{10}Be Muon Production Rate (atoms g^{-1} y^{-1})	^{26}Al Muon Production Rate (atoms g^{-1} y^{-1})	^{10}Be Spallation Rate (atoms g^{-1} y^{-1})	^{26}Al Spallation Rate (atoms g^{-1} y^{-1})	Total ^{10}Be production rate at depth (atoms g^{-1} y^{-1})	Total ^{26}Al production rate at depth (atoms g^{-1} y^{-1})
CF-02	7500	800	-200, +200	0.193	1.612	5.49	37.05	0.0745	0.6200
LC-02	7700	250	-50, +50	0.220	1.838	7.80	52.63	0.7559	5.3617
LC-04	7700	200	-50, +50	0.212	1.774	7.11	47.98	1.0719	7.5030
LC-05	7700	250	-50, +50	0.209	1.743	6.78	45.76	0.6702	4.7688
MC-01	8200	180	-30, +20	0.217	1.811	7.49	50.50	1.3468	9.3599
MC-02	12800	2000	-200, +200	0.181	1.513	4.54	30.61	0.0160	0.1334
GB-03	8000	700	-200, +200	0.185	1.540	4.82	32.52	0.0826	0.6822
GB-05	8000	300	-100, +100	0.211	1.759	6.96	46.94	0.4630	3.3559
SS-01	12800	550	-150, +50	0.181	1.511	4.50	30.39	0.1084	0.8800
SS-05	12800	3000	-500, +500	0.201	1.681	5.99	40.44	0.0053	0.0440

Deglaciation ages estimated based on proximity to dated moraine systems in Ullman et al., 2016 and Dalton et al., 2020 isochrons (see methods). Sample depth estimated in the field. Depth uncertainty estimated from photos and field journal and considered 95% confidence interval. Muonogenic and spallation surface production rates estimated from CRONUS online calculator using sample location data.

https://doi.org/10.5194/egusphere-2024-2233
Preprint. Discussion started: 29 July 2024
© Author(s) 2024. CC BY 4.0 License.

5. Results

^{10}Be and ^{26}Al were present above detection limits in 21 of 22 samples we analyzed, the one exception being the ^{26}Al measurement for sample GB-04, a modern stream sample (Tables 4 and 5, Figure 3). There is no significant difference between the measured concentrations of ^{10}Be for modern river sediment (mean and 1 SD = (3.31 ± 1.57) x 10^{4} atoms g^{-1}) and deglacial sediment ((2.25 ± 1.30) x 10^{4} atoms g^{-1}; Wilcoxon rank-sum test, p = 0.11). Similarly, there is no significant difference between the concentrations of ^{26}Al for modern ((2.12 ± 1.18) x 10^{5} atoms g^{-1}) and deglacial sediment ((1.47 ± 0.94) x 10^{5} atoms g^{-1}, p = 0.13). The single bedrock sample (GB-06) had the highest concentration of ^{10}Be ((7.33 ± 0.39) x 10^{4} atoms g^{-1}) and ^{26}Al ((5.91 ± 0.29) x 10^{5} atoms g^{-1}) that we measured.

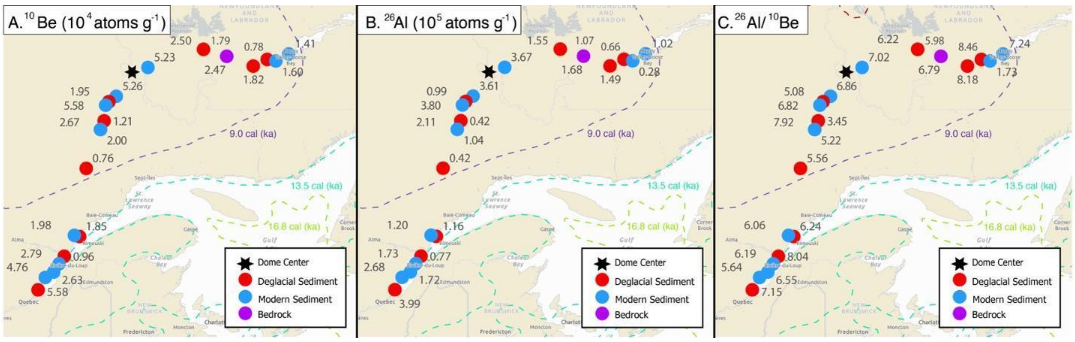

Figure 3. Maps showing isotopic data. A. Concentration of ^{10}Be. B. Concentration of ^{26}Al. C. ^{26}Al/^{10}Be ratio. Measured concentration plotted for modern sediment and bedrock and Holocene exposure-corrected concentration plotted for deglacial sediment. Sample identification shown in Figure 1B. Data in Tables 4 and 5. Sample type shown in key by color.

5.1. ^{10}Be and ^{26}Al Concentrations Corrected for Holocene Exposure

Using Holocene exposure-corrected data changes the results of statistical tests. With ^{10}Be, there was a significant difference between the concentrations of deglacial (mean and 1SD = (1.88 ± 1.40) x 10^{4} atoms g^{-1}) and modern ((3.31 ± 1.57) x 10^{4} atoms g^{-1}) samples (p = 0.02) (Figure 4A). For ^{26}Al, the concentration of deglacial ((1.21 ± 1.04) x 10^{5} atoms g^{-1}) and modern ((2.12 ± 1.18) x 10^{5} atoms g^{-1}) samples are also significantly different (p = 0.04) (Figure 4B). The modern samples have more ^{10}Be concentration variability, with an interquartile range (IQR) of 27.6 x 10^{3} atoms g^{-1} compared to the IQR of 8.2 x 10^{3} atoms g^{-1} for Holocene exposure-corrected deglacial samples. The bedrock sample (GB-06) contains 2.17 x10^{4} atoms g^{-1} of inherited ^{10}Be and 2.40 x 10^{5} atoms g^{-1} of inherited ^{26}Al.

5.2. ^{26}Al/^{10}Be Ratios

Using ^{10}Be and ^{26}Al concentrations from deglacial samples corrected for Holocene nuclide production, the error-weighted mean and standard deviation of ^{26}Al/^{10}Be ratios for deglacial and modern samples are 6.1 ± 1.2 and 6.6 ± 0.5, respectively (Figure 4C). Both a Wilcoxon rank-sum test (p = 0.63) and a Tukey HSD test (p = 0.84)

https://doi.org/10.5194/egusphere-2024-2233
Preprint. Discussion started: 29 July 2024
© Author(s) 2024. CC BY 4.0 License.

confirm that there is no significant difference between modern and deglacial sample $^{26}Al/^{10}Be$ ratios (Holocene corrected). The mean value for both is lower than the nominal production ratio at high latitudes. The ratios for deglacial samples are more variable (IQR = 2.37) compared to modern samples (IQR = 0.78). There is a significant, positive linear trend for deglacial samples, with ratio values increasing with distance from the center of the Quebec-Labrador Ice Dome ($r^2 = 0.45$, $p = 0.03$) (Figure 5). The five samples closest to the center of the ice dome (5.2 ± 0.8) have lower error-weighted average $^{26}Al/^{10}Be$ ratios than samples farther away (7.0 ± 0.7, Table 6 and Figure 6C). Modern samples, in contrast, exhibit no spatial trend in $^{26}Al/^{10}Be$ ratios. Tukey HSD tests (one including and excluding sample LC-04) show a significant difference between $^{26}Al/^{10}Be$ ratios in deglacial samples closest to and further from the center of the ice dome (both tests: $p = 0.00$).

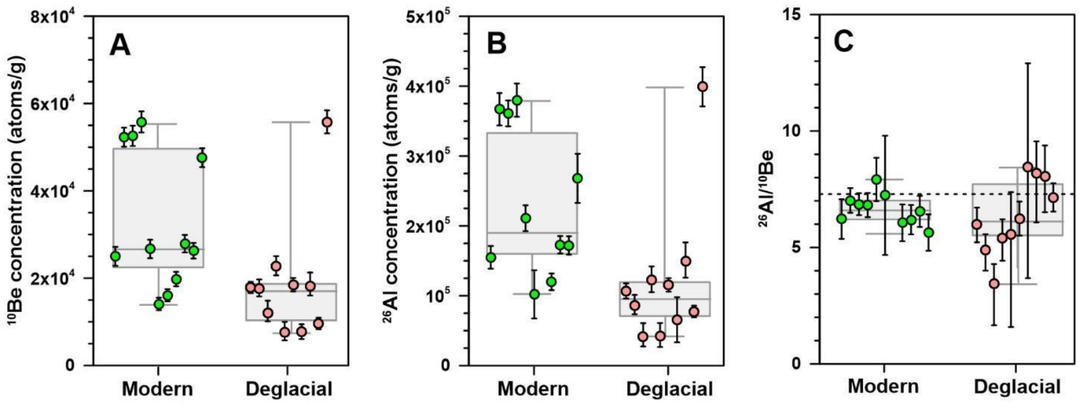

Figure 4. Comparison of modern and Holocene-exposure-corrected deglacial samples. (A) ^{10}Be concentrations, (B) ^{26}Al concentrations, and (C) $^{26}Al/^{10}Be$ ratios for deglacial (Holocene-corrected) and modern samples. The dashed line in panel C indicates the nominal production ratio (7.3) at high latitudes from Corbett et al. (2017). Points represent individual samples with 1σ propagated errors for modern (green) and deglacial (pink) samples. Box and whisker plots are shown for each dataset with whiskers going to the smallest and highest values. The box extends from the 25th to the 75th percentiles. The line in the middle of each box is the median.

https://doi.org/10.5194/egusphere-2024-2233
Preprint. Discussion started: 29 July 2024
© Author(s) 2024. CC BY 4.0 License.

Table 4. Measured Isotopic Data for ^{10}Be

Sample Name	Type	Quartz Mass (g)	Be Carrier Solution Mass (g)	Uncorrected ^{10}Be/^{9}Be Ratio [a]	Uncorrected ^{10}Be/^{9}Be Ratio Uncertainty [a]	Background Corrected ^{10}Be/^{9}Be Ratio	Background Corrected ^{10}Be/^{9}Be Ratio Uncertainty	Measured ^{10}Be (atoms g^{-1})	^{10}Be Uncertainty (atoms g^{-1})	Cathode #
CF-02	Deglacial	20.46	0.7353	2.31×10^{-14}	1.55×10^{15}	2.23×10^{-14}	1.58×10^{15}	1.84×10^{4}	1.30×10^{3}	169432
LC-02	Deglacial	21.95	0.7364	3.11×10^{-14}	1.87×10^{15}	3.04×10^{-14}	1.89×10^{15}	2.34×10^{4}	1.45×10^{3}	169436
LC-04	Deglacial	19.74	0.7348	2.45×10^{-14}	1.54×10^{15}	2.38×10^{-14}	1.57×10^{15}	2.04×10^{4}	1.34×10^{3}	169438
LC-05	Deglacial	19.29	0.7348	3.26×10^{-14}	2.13×10^{15}	3.18×10^{-14}	2.15×10^{15}	2.79×10^{4}	1.88×10^{3}	169439
MC-01	Deglacial	19.60	0.7342	2.24×10^{-14}	1.85×10^{15}	2.17×10^{-14}	1.88×10^{15}	1.86×10^{4}	1.61×10^{3}	169441
MC-02	Deglacial	18.75	0.7319	2.16×10^{-14}	1.69×10^{15}	2.09×10^{-14}	1.71×10^{15}	1.87×10^{4}	1.54×10^{3}	169442
GB-03	Deglacial	9.38	0.7353	5.42×10^{-15}	8.92E-16	4.68×10^{-15}	9.35E-16	8.42×10^{3}	1.68×10^{3}	169444
GB-05	Deglacial	20.10	0.7310	2.70×10^{-14}	2.37×10^{15}	2.62×10^{-14}	2.39×10^{15}	2.19×10^{4}	1.99×10^{3}	169447
SS-01	Deglacial	19.70	0.7337	1.36×10^{-14}	1.48×10^{15}	1.28×10^{-14}	1.50×10^{15}	1.10×10^{4}	1.29×10^{3}	169450
SS-05	Deglacial	20.88	0.7308	7.02×10^{-14}	3.26×10^{15}	6.95×10^{-14}	3.28×10^{15}	5.59×10^{4}	2.63×10^{3}	169454
CF-01	Modern	18.52	0.7331	2.82×10^{-14}	2.37×10^{15}	2.75×10^{-14}	2.39×10^{15}	2.50×10^{4}	2.17×10^{3}	169431
CF-05	Modern	20.92	0.7348	6.55×10^{-14}	2.69×10^{15}	6.48×10^{-14}	2.71×10^{15}	5.23×10^{4}	2.18×10^{3}	169434
LC-01	Modern	20.41	0.7330	6.44×10^{-14}	2.81×10^{15}	6.37×10^{-14}	2.83×10^{15}	5.26×10^{4}	2.33×10^{3}	169435
LC-03	Modern	20.50	0.7307	6.88×10^{-14}	2.93×10^{15}	6.81×10^{-14}	2.94×10^{15}	5.58×10^{4}	2.41×10^{3}	169437
LC-06	Modern	19.44	0.7345	3.14×10^{-14}	2.42×10^{15}	3.07×10^{-14}	2.44×10^{15}	2.67×10^{4}	2.12×10^{3}	169440
GB-02	Modern	19.96	0.7311	1.75×10^{-14}	1.65×10^{15}	1.68×10^{-14}	1.67×10^{15}	1.41×10^{4}	1.41×10^{3}	169443
GB-04	Modern	17.34	0.7362	1.72×10^{-14}	1.39×10^{15}	1.65×10^{-14}	1.42×10^{15}	1.61×10^{4}	1.39×10^{3}	169445
MC-03	Modern	20.73	0.7304	2.51×10^{-14}	2.03×10^{15}	2.44×10^{-14}	2.05×10^{15}	1.98×10^{4}	1.66×10^{3}	169449
SS-02	Modern	20.37	0.7345	3.44×10^{-14}	2.41×10^{15}	3.37×10^{-14}	2.43×10^{15}	2.79×10^{4}	2.01×10^{3}	169451
SS-03	Modern	20.81	0.7349	3.31×10^{-14}	2.17×10^{15}	3.24×10^{-14}	2.19×10^{15}	2.63×10^{4}	1.78×10^{3}	169452
SS-04	Modern	22.15	0.7349	6.31×10^{-14}	2.82×10^{15}	6.24×10^{-14}	2.83×10^{15}	4.76×10^{4}	2.16×10^{3}	169453

https://doi.org/10.5194/egusphere-2024-2233
Preprint. Discussion started: 29 July 2024
© Author(s) 2024. CC BY 4.0 License.

GB-06	Bedrock	15.35	0.7365	6.73×10^{-14}	3.53×10^{15}	6.65×10^{-14}	3.54×10^{15}	7.33×10^{4}	3.90×10^{3}	169448

[a] Isotopic analysis conducted at PRIME Laboratory; ratios were normalized against standard 07KNSTD3110 with an assumed ratio of 2850×10^{-15} (Nishiizumi et al., 2007).

All uncertainties are 1σ.

https://doi.org/10.5194/egusphere-2024-2233
Preprint. Discussion started: 29 July 2024
© Author(s) 2024. CC BY 4.0 License.

381 **Table 5. Measured Isotopic Data for ^{26}Al**

Sample Name	Type	Quartz Mass (g)	Total ^{27}Al Quantified by ICP-OES (μg)[a]	Uncorrected $^{26}Al/^{27}Al$ Ratio [b]	Uncorrected $^{26}Al/^{27}Al$ Ratio Uncertainty [b]	Background Corrected $^{26}Al/^{27}Al$ Ratio	Background Corrected $^{26}Al/^{27}Al$ Ratio Uncertainty	Measured ^{26}Al (atoms g^{-1})	^{26}Al Uncertainty (atoms g^{-1})	Measured $^{26}Al/^{10}Be$	$^{26}Al/^{10}Be$ Uncertainty	Cathode #
CF-02	Deglacial	20.46	3394	3.07×10^{14}	2.91×10^{15}	3.01×10^{14}	2.91×10^{15}	1.12×10^{5}	1.08×10^{4}	6.05	0.72	169432
LC-02	Deglacial	21.95	1682	7.50×10^{14}	6.25×10^{15}	7.45×10^{14}	6.25×10^{15}	1.27×10^{5}	1.07×10^{4}	5.44	0.57	169436
LC-04	Deglacial	19.74	1882	4.73×10^{14}	4.80×10^{15}	4.67×10^{14}	4.80×10^{15}	9.94×10^{4}	1.02×10^{4}	4.89	0.60	169438
LC-05	Deglacial	19.29	3401	4.11×10^{14}	4.24×10^{15}	4.05×10^{14}	4.24×10^{15}	1.60×10^{5}	1.67×10^{4}	5.72	0.71	169439
MC-01	Deglacial	19.60	5255	2.04×10^{14}	2.39×10^{15}	1.99×10^{14}	2.39×10^{15}	1.19×10^{5}	1.43×10^{4}	6.38	0.95	169441
MC-02	Deglacial	18.75	1757	5.66×10^{14}	4.57×10^{15}	5.61×10^{14}	4.57×10^{15}	1.17×10^{5}	9.56×10^{3}	6.27	0.73	169442
GB-03	Deglacial	9.38	7435	4.56×10^{15}	1.83×10^{15}	4.02×10^{15}	1.83×10^{15}	7.11×10^{4}	3.23×10^{4}	8.44	4.19	169444
GB-05	Deglacial	20.10	5364	3.01×10^{14}	3.74×10^{15}	2.95×10^{14}	3.74×10^{15}	1.76×10^{5}	2.23×10^{4}	8.02	1.25	169447
SS-01	Deglacial	19.70	1512	5.22×10^{14}	4.66×10^{15}	5.16×10^{14}	4.66×10^{15}	8.84×10^{4}	7.98×10^{3}	8.05	1.19	169450
SS-05	Deglacial	20.88	3437	1.09×10^{13}	7.64×10^{15}	1.09×10^{13}	7.64×10^{15}	3.99×10^{5}	2.81×10^{4}	7.15	0.61	169454
CF-01	Modern	18.52	2977	4.39×10^{14}	4.56×10^{15}	4.33×10^{14}	4.56×10^{15}	1.55×10^{5}	1.63×10^{4}	6.22	0.85	169431
CF-05	Modern	20.92	3327	1.04×10^{13}	6.54×10^{15}	1.03×10^{13}	6.54×10^{15}	3.67×10^{5}	2.32×10^{4}	7.02	0.53	169434
LC-01	Modern	20.41	2056	1.61×10^{13}	8.24×10^{15}	1.60×10^{13}	8.24×10^{15}	3.61×10^{5}	1.85×10^{4}	6.86	0.47	169435
LC-03	Modern	20.50	2013	1.74×10^{13}	1.09E-14	1.73×10^{13}	1.09×10^{14}	3.80×10^{5}	2.38×10^{4}	6.82	0.52	169437
LC-06	Modern	19.44	2743	6.76×10^{14}	5.83×10^{15}	6.70×10^{14}	5.83×10^{15}	2.11×10^{5}	1.84×10^{4}	7.92	0.93	169440
GB-02	Modern	19.96	20382	5.02×10^{15}	1.52×10^{15}	4.48×10^{15}	1.52×10^{15}	1.02×10^{5}	3.46×10^{4}	7.24	2.56	169443
GB-04	Modern	17.34	17148	1.80×10^{15}	1.20×10^{15}	1.26×10^{15}	1.20×10^{15}	Below Detection Limit	Below Detection Limit	----	----	169445
MC-03	Modern	20.73	1806	6.21×10^{14}	6.10×10^{15}	6.16×10^{14}	6.10×10^{15}	1.20×10^{5}	1.19×10^{4}	6.06	0.79	169449
SS-02	Modern	20.37	1837	8.63×10^{14}	6.19×10^{15}	8.58×10^{14}	6.19×10^{15}	1.73×10^{5}	1.25×10^{4}	6.19	0.63	169451
SS-03	Modern	20.81	3229	5.02×10^{14}	3.79×10^{15}	4.97×10^{14}	3.80×10^{15}	1.72×10^{5}	1.31×10^{4}	6.55	0.67	169452
SS-04	Modern	22.15	8285	3.27×10^{14}	4.20×10^{15}	3.22×10^{14}	4.21×10^{15}	2.68×10^{5}	3.51×10^{4}	5.64	0.78	169453

https://doi.org/10.5194/egusphere-2024-2233
Preprint. Discussion started: 29 July 2024
© Author(s) 2024. CC BY 4.0 License.

GB-06	Bedrock	15.35	2509	1.62×10^{13}	7.95×10^{15}	1.62×10^{13}	7.95×10^{15}	5.91×10^{5}	2.90×10^{4}	8.05	0.58	169448

[a] ^{27}Al was added only to samples with insufficient total Al through commercial SPEX ICP standard with a concentration of 1000 μg mL^{-1}. The total here reflects the sum of Al added through carrier and native Al in quartz.

[b] Isotopic analysis conducted at PRIME Laboratory; ratios were normalized against standard KNSTD with an assumed ratio of 1.818×10^{-12} (Nishiizumi et al., 2004).

All uncertainties are 1σ.

https://doi.org/10.5194/egusphere-2024-2233
Preprint. Discussion started: 29 July 2024
© Author(s) 2024. CC BY 4.0 License.

Table 6. Holocene Corrected Concentrations for Deglacial Samples

Sample Name	Type of Deposit	Distance from Labrador City (km)	Inherited ^{10}Be (atoms g^{-1})	^{10}Be Uncertainty (atoms g^{-1}) [a]	Inherited ^{26}Al (atoms g^{-1})	^{26}Al Uncertainty (atoms g^{-1}) [a]	^{26}Al/^{10}Be at Time of Deposition	^{26}Al/^{10}Be Uncertainty [a]
LC-02	esker	109	1.76×10^4	$(-2.15, +1.74) \times 10^3$	8.61×10^4	$(-1.51, +1.25) \times 10^4$	4.90	-0.88, +0.67
LC-04	ice contact fan	162	1.21×10^4	$(-2.74, +1.97) \times 10^3$	4.17×10^4	$(-1.91, +1.41) \times 10^4$	3.45	-1.79, +0.84
LC-05	outwash fan	188	2.27×10^4	$(-2.33, +2.06) \times 10^3$	1.23×10^5	$(-1.91, +1.76) \times 10^4$	5.41	-0.97, +0.81
CF-02	glacial delta	221	1.79×10^4	$(-1.31, +1.30) \times 10^3$	1.07×10^5	$(-1.08, +1.08) \times 10^4$	5.98	-0.75, +0.74
MC-01	esker or outwash fan	309	7.60×10^3	$(-2.39, +1.85) \times 10^3$	4.23×10^4	$(-1.86, +1.56) \times 10^4$	5.56	-3.98, +1.81
GB-05	esker	361	1.82×10^4	$(-3.09, +2.18) \times 10^3$	1.49×10^5	$(-2.74, +2.31) \times 10^4$	8.18	-2.10, +1.38
GB-03	glacial delta	403	7.76×10^3	$(-1.69, +1.68) \times 10^3$	6.56×10^4	$(-3.23, +3.23) \times 10^4$	8.46	-4.78, +4.45
MC-02	glacial delta	506	1.85×10^4	$(-1.54, +1.54) \times 10^3$	1.16×10^5	$(-9.56, +9.56) \times 10^3$	6.24	-0.73, +0.73
SS-01	glacial delta	580	9.59×10^3	$(-1.37, +1.29) \times 10^3$	7.72×10^4	$(-8.71, +8.00) \times 10^3$	8.04	-1.53, +1.34
SS-05	glacial delta	710	5.58×10^4	$(-2.63, +2.63) \times 10^3$	3.99×10^5	$(-2.81, +2.81) \times 10^4$	7.15	-0.61, +0.61

[a] Uncertainty for both nuclides was calculated by propagating error from AMS data reduction with depth estimation error (see methods). Depth estimate uncertainty and changing production rates with depth create asymmetrical uncertainty in both nuclide concentrations. All uncertainties are 1σ.

https://doi.org/10.5194/egusphere-2024-2233
Preprint. Discussion started: 29 July 2024
© Author(s) 2024. CC BY 4.0 License.

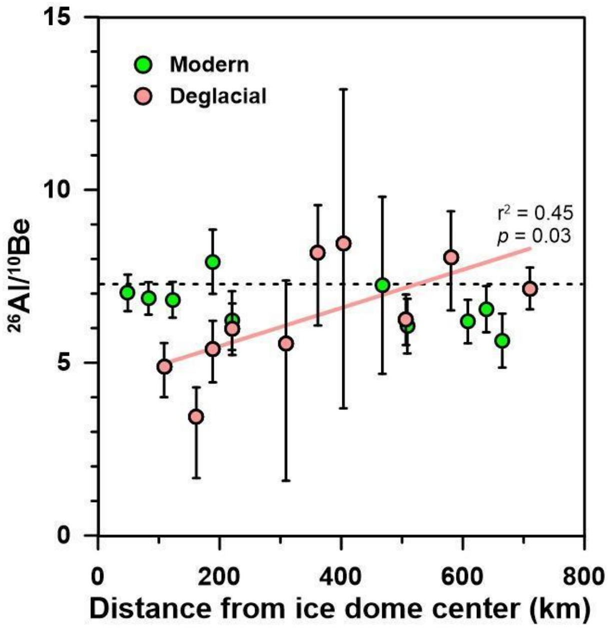

Figure 5. $^{26}Al/^{10}Be$ ratios versus distance from center of the Quebec-Labrador Ice Dome at Labrador City. Deglacial data are corrected for Holocene nuclide production and fit with a trendline. Error bars are1σ. Dashed line shows production ratio at high latitudes (7.3) (Corbett et al., 2017).

6. Discussion

Measurements of in situ produced ^{10}Be and ^{26}Al in sediment and bedrock sampled in eastern Quebec and in Labrador indicate that LIS erosion and sediment transport during the last glacial period were not sufficient to remove all cosmogenic nuclides accumulated during previous periods of exposure (Figure 4A,B). Corrected for Holocene exposure, the error-weighted mean $^{26}Al/^{10}Be$ for both deglacial (6.1 ± 1.2) and modern fluvial sediments (6.6 ± 0.5) are lower than the production ratio of the two nuclides at high latitudes (7.3 ± 0.3) (Corbett et al., 2017) (Figure 6A-C), consistent with burial after initial exposure. A Tukey HSD test confirms a significant difference between our deglacial (Holocene corrected) $^{26}Al/^{10}Be$ ratios and the 7.3 ± 0.3 production ratio ($p = 0.01$). However, most of these terrestrial samples have $^{26}Al/^{10}Be$ ratios higher than those (4.7 ± 0.8) measured in North Atlantic quartz IRD thought to be sourced from northeastern Canada (LeBlanc et al., 2023) (Figure 6D). Together these data suggest that the IRD measured by LeBlanc et al. was either not sourced from much of eastern Quebec and Labrador that we sampled or was buried beyond the depth of cosmic-ray penetration for hundreds of thousands of years (in Hudson Bay or thick sediment deposits) before being transported as IRD.

https://doi.org/10.5194/egusphere-2024-2233
Preprint. Discussion started: 29 July 2024
© Author(s) 2024. CC BY 4.0 License.

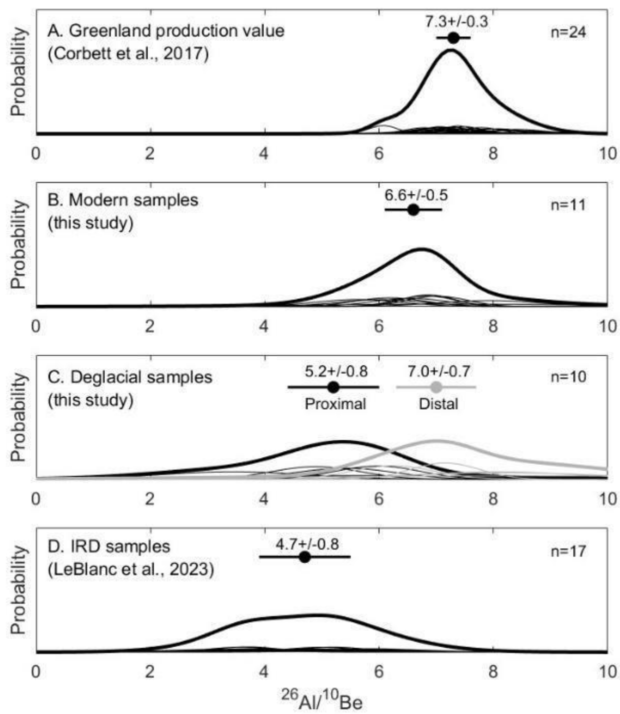

Figure 6. Summed probability plots of $^{26}Al/^{10}Be$ ratios for Arctic samples. A. Samples with simple exposure histories in Greenland (Corbett et al., 2017). B. Modern stream sediment (this study). C. Deglacial samples corrected for Holocene exposure; black 5 samples most proximal to Labrador City (center of the dome); gray 5 samples are most distal (this study). D. IRD samples from North Atlantic (LeBlanc et al, 2023). Analytical error weighted mean and 1 SD uncertainty above each plot.

6.1 Nuclide Concentrations in Deglacial Sediments Indicate Limited Erosion by Laurentide Ice

After correcting for Holocene exposure, all deglacial sediment samples in our study (n = 10) contain ^{26}Al and ^{10}Be inherited from exposure during prior interglacials. The center of the Quebec-Labrador Ice Dome was covered by ice starting at least ~70 ka and as early as ~115 ka and did not deglaciate until 7 ka (Ullman et al., 2016; Dalton et al., 2022). Despite being buried for ~60-105 ka by the LIS during the last glacial period, nuclide concentrations in sediment (and at least some bedrock) have not been reset by erosion to zero. The average inherited ^{10}Be concentration (1.88×10^4 atoms g^{-1}) is equivalent to ~3,000 years of surface production, assuming the average production rate across the sites (6.35 atoms g^{-1} yr^{-1}). If these nuclides were produced during last interglacial exposure (poorly constrained to between 10 and 60 kyr in the center of our transect) the implied eroded depth would be a few meters over tens of thousands to perhaps one hundred thousand years – a low average rate of erosion.

https://doi.org/10.5194/egusphere-2024-2233
Preprint. Discussion started: 29 July 2024
© Author(s) 2024. CC BY 4.0 License.

Subglacial process modeling over North America supports a minimally erosive LIS in portions of Quebec and Labrador during the last glacial cycle (Melanson et al., 2013) consistent with our findings. Specifically, Melanson et al.'s modeling of the Quebec-Labrador region exhibits minima for both basal sliding speed and total ice movement integrated over the last glacial cycle – both variables related to the efficacy of glacial erosion. Simulated ice sliding distances (the integrated basal velocity over the last glacial cycle in millions of meters (Mm)) are near zero in the center of our study area, 1 Mm near Goose Bay, and 3 Mm along the St. Lawrence estuary – an order of magnitude less than for the Hudson Strait ice stream and southern LIS lobes (Melanson et al., 2013). Total erosion predicted using empirical abrasion and quarrying laws ranges from near zero under the center of the Quebec-Labrador dome to ≥10 m along parts of its Atlantic and St. Lawrence margin. Our data are consistent with a variably erosive LIS, which contained regions of slow ice movement and thus insignificant erosion where nuclides from prior periods of exposure are more likely to have been retained. This pattern may help explain the patchy and thin sediment cover present in Quebec and Labrador today (Pelletier et al., 2016).

Our results agree with ^{10}Be measurements made by others in bedrock and boulders sampled to date deglacial landforms in Quebec and Labrador. The bedrock sample we analyzed (GB-06), which contained ^{10}Be inheritance equivalent to ~3.2 ka of surface exposure, was collected adjacent to samples CL3-10-01 (1.1 km from GB-06) and CL3-10-07 (0.7 km from GB-06) both along Ullman et al.'s (2016) CL3 transect. Ullman et al. excluded these boulder samples from their deglacial chronology because their estimated ages (14.2 and 12.4 ka) were deemed much too old. In total, 10 of 65 boulder samples from Ullman et al.'s (2016) southern and eastern transects, which overlap our transect, were regarded as outliers because of their unusually high concentration of ^{10}Be. Couette et al. (2023) similarly excluded 5 of 37 samples in eastern Labrador because of high ^{10}Be concentrations. The results suggest inheritance from prior exposure is common in boulders and bedrock in the region.

The concentrations of inherited nuclides we measured in LIS deglacial sediment (~19,000 ^{10}Be atoms g^{-1}) are on average several times higher than those currently in sediment shed by the Greenland Ice Sheet (~6,500 ^{10}Be atoms g^{-1}, Nelson et al., 2014) but much lower than those deposited by the LIS in the midwestern United States (~60,000 ^{10}Be atoms g^{-1}, Balco et al., 2005). Nuclide concentrations in deglacial sediment must reflect a combination of interglacial exposure duration, glacial erosivity, and nuclide decay during burial. The low concentrations of ^{10}Be in sediment issuing from the Greenland Ice Sheet (as well as low $^{26}Al/^{10}Be$ ratios ~4.5, Bierman et al., 2016) reflect continuous ice cover through most interglacials and erosive warm-based ice in areas from which sediment is sourced. In contrast, the high concentrations of ^{10}Be in deglacial sediment originating from the southern margin of the Keewatin Ice Dome in Minnesota (Balco et al., 2005) suggest that ice there, although it lingered through many interglacials to provide low $^{26}Al/^{10}Be$ ratios (also ~4.5), was only weakly erosive and thus perhaps at least in part, cold-based.

6.2 Implications for Cosmogenic Dating

Our findings of nuclide inheritance from prior periods of exposure, and thus limited glacial erosion, are consistent with studies conducted in other regions of the LIS, as well as glacial and deglacial landscapes in Fennoscandia and Greenland (e.g., Stroeven et al., 2002; Corbett et al., 2016; Briner & Swanson, 1998). Our data, as well as those of others, have implications for the use of in situ produced cosmogenic nuclides for both exposure and burial dating.

Measurements in several other parts of the LIS have shown that boulders, cobbles, and sand carried nuclides inherited from prior periods of surface exposure. For example, a cobble sampled from Baffin Island had concentrations of ^{10}Be and ^{26}Al that suggested nuclide inheritance equivalent to ~3 ka years of surface exposure (Davis et al., 1999). In the northeastern United States, Halsted et al. (2023) estimated that boulders on LIS terminal moraines contained concentrations of inherited ^{10}Be equivalent to 2-6 ka of surface exposure. In the midwestern United States, the ^{26}Al/^{10}Be ratio was well below the production value in glacial outwash negating efforts to use older deposits for burial dating (Balco et al., 2005). In the Torngat Mountains of northern Labrador, measurements of ^{26}Al and ^{10}Be on bedrock sites and erratic boulders at mountain summits provide evidence of minimal erosion (<1.4 m Ma^{-1}) where cold-based ice was predominant before deglaciation (Staiger et al., 2005). In south-central Wisconsin, three out of five bedrock outcrops sampled had concentrations of ^{10}Be and ^{26}Al eight times higher than predicted based on radiocarbon dating (Colgan et al., 2002).

Minimal erosion and significant inheritance of cosmogenic nuclides have been observed in areas once occupied by other Northern Hemisphere ice sheets as well. On the historical periphery of the Scandinavian Ice Sheet (southwestern Norway), glacial erratic boulders had the surface equivalent of ~2 ka years of inherited muonogenic ^{10}Be (Briner et al., 2016). Towards the center of that ice sheet (northeastern Sweden) there is evidence that bedrock outcrops and boulder fields have been preserved through many glacial cycles since the late Cenozoic (Stroeven et al., 2002). There is also evidence of minimal erosion near the margin of the Cordilleran Ice Sheet, with 8 out of 23 bedrock samples on Whitbey Island having ^{36}Cl/Cl ratios suggesting inheritance of nuclides produced from prior interglacials (Briner & Swanson, 1998). In northwest Greenland, 8 of 28 sampled boulders had high concentrations of ^{10}Be and ^{26}Al along with low ^{26}Al/^{10}Be ratios indicative of burial, providing evidence of minimal subglacial erosion over multiple interglacial and glacial periods where the ice was predominantly cold-based (Corbett et al., 2016).

The inheritance of nuclides from prior periods of exposure has implications for cosmogenic exposure dating of bedrock outcrops, boulders, and sediment deposits, because nuclide concentrations are biased too high. For example, Ullman et al. (2016) noted that their ^{10}Be-based deglacial chronology in our study area leads radiocarbon-based estimates of local deglaciation by centuries (see their Figure 7). While radiocarbon lags are frequently attributed to delayed colonization of the landscape by vegetation following deglaciation (e.g., Peteet et al., 2012), the widespread nuclide inheritance we find in Quebec-Labrador suggests that, at least in this case, it is the ^{10}Be ages that may be too old. Practical solutions include larger sample sizes to facilitate outlier identification, sampling shielded material as we have done to quantify the magnitude of nuclide inheritance, and the application of short-lived nuclides such as in situ ^{14}C which, because of its half-life (5730 years) does not retain nuclides from prior interglaciations (e.g., Hippe, 2017).

https://doi.org/10.5194/egusphere-2024-2233
Preprint. Discussion started: 29 July 2024
© Author(s) 2024. CC BY 4.0 License.

6.3 The Quebec-Labrador Ice Dome Center Persisted During Some Interglacials

Finding $^{26}Al/^{10}Be$ ratios below production in quartz IRD from North Atlantic Heinrich layers, LeBlanc et al. (2023) concluded that ice sheet remnants must have lingered in parts of eastern Canada for the majority of Pleistocene interglacials. While Heinrich layer sediment was predominantly delivered to the ocean by the Hudson Strait ice stream, the quartz IRD LeBlanc et al. (2023) analyzed most likely came from interior areas of the LIS feeding the ice stream because Hudson Strait is underlain primarily by carbonate rocks (Bond et al., 1992).

Data we present in this paper suggest that the quartz analyzed by LeBlanc et al. (2023) could have been sourced from parts our field area near Labrador City because only there are $^{26}Al/^{10}Be$ ratios of the Holocene-corrected deglacial sediment like those in the IRD (Figure 6C, D). Alternatively, it is possible that IRD was sourced from a wider area (the Keewatin Dome and/or Baffin Island) where samples of sediment (Balco et al., 2005) and taken from outcrops (Marsella et al., 2002) have low $^{26}Al/^{10}Be$ ratios. It is also possible that sediment was stored in Hudson Bay for ~1 Ma, where ^{26}Al and ^{10}Be decayed, before being transported to the deep sea.

Sediment could have also been recycled multiple times on land and shielded from interglacial exposure in thick deposits (e.g., deltas) before eventually making it to the ocean as IRD. This lag between initial deposition, either in Hudson Bay or in thick sedimentary sequences on land, and final transport by ice into the Atlantic Ocean allows for the sediment to have initially had higher ratios of $^{26}Al/^{10}Be$ (like the range of ratios in our deglacial data). The low rates of glacial erosion and ice sliding in this region suggested by our data as well as models (Melanson et al., 2013) could help account for such long residence times of terrestrial sediment in Quebec-Labrador; yet, the absence of lower than production $^{26}Al/^{10}Be$ ratios in deglacial sediment closer to the ice sheet margin remains inconsistent with long term burial. Perhaps incorporation of IRD occurred primarily toward the center of the ice sheet and not closer to the margins.

Although we cannot say during which interglacials the Quebec-Labrador Ice Dome remained in a reduced state and during which it completely melted like it has today, the inverse relationship between $^{26}Al/^{10}Be$ sample ratios and distance from the center of the dome at present-day Labrador City provides strong evidence that ice lingered in that area for at least some interglacial periods shielding rock and sediment below from cosmic rays. In contrast, the higher $^{26}Al/^{10}Be$ ratios in deglacial sediment further from the center of the ice dome are consistent with repeated exposure during interglacials. More extensive sampling of eastern Canada, including Quebec-Labrador, and further north near Hudson Bay and Baffin Island, would provide further evidence on how persistent different sectors of the eastern LIS was during Pleistocene interglacials.

6.3 Sediment Sourcing in Modern Rivers

We can estimate the percentage of sediment derived from erosion of deglacial materials using a two component, linear mixing model based on the measured concentrations of ^{10}Be in both river and deglacial sediment and assumptions about nuclide production since deglaciation. One component is deglacial deposits which, based on our sampling today, contain an average of 22.5 x 10^3 ^{10}Be atoms g^{-1} and enter rivers by bank incision (Figure 4A). The second component is surficial materials which, when eroded, enter the drainage network. Since we did not

https://doi.org/10.5194/egusphere-2024-2233
Preprint. Discussion started: 29 July 2024
© Author(s) 2024. CC BY 4.0 License.

sample these surficial materials directly, we calculate their ^{10}Be concentration by assuming that at the time of deglaciation (the beginning of exposure) surface sediment contained the average Holocene exposure-corrected concentration of ^{10}Be for deglacial sediment (18.7 x 10^3 ^{10}Be atoms g^{-1}). We then use the average deglacial age of 9.32 ka for our field area and the average ^{10}Be surface production rate (7.82 atoms y^{-1} g^{-1}) to calculate that surface material gained about 7.3 x 10^4 ^{10}Be atoms g^{-1} since deglaciation. The surface-exposed end member therefore contains 91.6 x10^3 ^{10}Be atoms g^{-1}.

Knowing that modern sediment contains on average 33.1 x 10^3 ^{10}Be atoms g^{-1}, the two-component mixing model suggests that about 85% of sediment in eastern Quebec rivers today is derived from incision of glacial deposits and only about 15% comes from erosion of surficial sediment and bedrock. Our findings for eastern Quebec are like those of Balco et al. (2005) in Minnesota. In that previously glaciated region, they suggest most sediment carried by rivers comes from incision of glacial deposits. Our finding is also consistent with the low sediment yield of forested upland terrains in other glaciated areas of the LIS (e.g., Dethier et al., 2018).

Conclusions

Analysis of cosmogenic ^{10}Be and ^{26}Al in deglacial (n=10) and modern (n=11) sediment samples indicates that the Quebec-Labrador Ice Dome was minimally erosive during the last glacial period, allowing preservation of nuclides created during prior interglacial exposures. Nuclide concentrations in modern sediments are only slightly higher than those in deglacial sediments on average, implying most sediment transported by rivers today is sourced from rapidly eroding banks composed of glacial deposits rather than surrounding slowly-eroding surfaces. Holocene exposure-corrected ratios of ^{26}Al/^{10}Be in deglacial samples are below the production ratio of those nuclides at high latitudes near the center of the ice dome but not the margins, implying interior ice survived during at least some interglacials but peripheral ice did not. Further sampling of this region and northward near the Foxe-Baffin and Keewatin Domes may provide more evidence of minimal erosion and show if and where ice persisted during Pleistocene interglacials. Such data are important both for understanding the lower than production ^{26}Al/^{10}Be ratios measured in IRD from eastern LIS discharge and for determining the interglacial history of the LIS.

Author contribution

Cavnar drafted and edited the manuscript and performed data reduction and statistical analysis. Cavnar and Shakun collected samples in the field. Bierman and Shakun are responsible for study conception and design. Bierman and Shakun edited the manuscript and advised Cavnar on sample preparation and data analysis. Cavnar performed sample cleaning and extraction under the supervision of Corbett. Corbett, Galford, and LeBlanc edited figures coded by Cavnar and assisted with conceptual design of figures and manuscript organization. Caffee assisted with statistical analysis and oversaw measurement of cosmogenic nuclides via AMS and PRIME Lab.

Competing Interests

The authors declare that they have no conflict of interest.

© Author(s) 2024. CC BY 4.0 License.

Acknowledgements

We thank the 2022 field sampling team including Juliana Souza, Halley Mastro, and Cat Collins. We appreciate help from Pierre-Olivier Couette and Patrick Lajeunesse to identify sample locations. Funding for this research was provided by NSF-EAR-2300560, 2116209, and 1735676 awards to Bierman and Corbett, and 2116208 to Shakun.

References

Abe-Ouchi, A., Saito, F., Kawamura, K., Raymo, M. E., Okuno, J., Takahashi, K., & Blatter, H. (2013). Insolation-driven 100,000-year glacial cycles and hysteresis of ice-sheet volume. *Nature*, *500*(7461), 190–193. https://doi.org/10.1038/nature12374

Amani, M., Mahdavi, S., Afshar, M., Brisco, B., Huang, W., Mirzadeh, S. M. J., White, L., Banks, S. N., Montgomery, J., & Hopkinson, C. (2019). Canadian Wetland Inventory using Google Earth Engine: The First Map and Preliminary Results. *Remote Sensing*, *11*(7), 842. https://doi.org/10.3390/rs11070842

Andrews, J. T., & Tyler, K. L. (2011). The observed postglacial recovery of Québec and Nouveau-Québec Since 12,000 BP. *Géographie Physique Et Quaternaire*, *31*(3–4), 389–400. https://doi.org/10.7202/1000286ar

Applegate, P. J., Urban, N. M., Laabs, B. J. C., Keller, K., and Alley, R. B.: Modeling the statistical distributions of cosmogenic exposure dates from moraines, Geosci. Model Dev., 3, 293–307, https://doi.org/10.5194/gmd-3-293-2010, 2010.

Balco, G., Stone, J. O. H., & Jennings, C. (2005). Dating Plio-Pleistocene glacial sediments using the cosmic-ray-produced radionuclides ^{10}Be and ^{26}Al. *American Journal of Science*, *305*(1), 1–41. https://doi.org/10.2475/ajs.305.1.1

Batchelor, C. L., Margold, M., Krapp, K., Murton, D. K., Dalton, A. S., Gibbard, P. L., Stokes, C. R., Murton, J. B., & Manica, A. (2019). The configuration of Northern Hemisphere ice sheets through the Quaternary. *Nature Communications, 10.* https://doi.org/10.1038/s41467-019-11601-2

Beck, H. E., Zimmermann, N. E., McVicar, T. R., Vergopolan, N., Berg, A., & Wood, E. F. (2018). Present and future Köppen-Geiger climate classification maps at 1-km resolution. *Scientific Data*, *5*(1). https://doi.org/10.1038/sdata.2018.214

Bierman, P. (1994). Using in situ produced cosmogenic isotopes to estimate rates of landscape evolution: A review from the geomorphic perspective. *Journal of Geophysical Research, 99*(10), 13.885-13.896

Bierman, P. R., Marsella, K. A., Patterson, C. J., Davis, P. T., & Caffee, M. W. (1999). Mid-Pleistocene cosmogenic minimum-age limits for pre-Wisconsinan glacial surfaces in southwestern Minnesota and southern Baffin Island: a multiple nuclide approach. *Geomorphology*, *27*(1–2), 25–39. https://doi.org/10.1016/s0169-555x(98)00088-9

Bierman, P. R., Shakun, J. D., Corbett, L. B., Zimmerman, S., & Rood, D. H. (2016). A persistent and dynamic East Greenland Ice Sheet over the past 7.5 million years. *Nature*, *540*(7632), 256–260. https://doi.org/10.1038/nature20147

Bintanja, R., & Van De Wal, R. S. W. (2008). North American ice-sheet dynamics and the onset of 100,000-year glacial cycles. *Nature*, *454*(7206), 869–872. https://doi.org/10.1038/nature07158

Braucher, R., Brown, E. T., Bourlès, D., & Colin, F. (2003). In situ produced ^{10}Be measurements at great depths: implications for production rates by fast muons. *Earth and Planetary Science Letters*, *211*(3–4), 251–258. https://doi.org/10.1016/s0012-821x(03)00205-x

Braucher, R., Merchel, S., Borgomano, J., & Bourlès, D. (2011). Production of cosmogenic radionuclides at great depth: A multi element approach. *Earth and Planetary Science Letters*, *309*(1–2), 1–9. https://doi.org/10.1016/j.epsl.2011.06.036

Briner, J. P., Goehring, B. M., Mangerud, J., & Svendsen, J. I. (2016). The deep accumulation of 10Be at Utsira, southwestern Norway: Implications for cosmogenic nuclide exposure dating in peripheral ice sheet landscapes. *Geophysical Research Letters*, *43*(17), 9121–9129. https://doi.org/10.1002/2016gl070100

Briner, J. P., & Swanson, T. W. (1998). Using inherited cosmogenic ^{36}Cl to constrain glacial erosion rates of the Cordilleran ice sheet. *Geology* | *GeoScienceWorld*. https://doi.org/10.1130/0091-7613(1998)026

https://doi.org/10.5194/egusphere-2024-2233
Preprint. Discussion started: 29 July 2024
© Author(s) 2024. CC BY 4.0 License.

Colgan, P. M., Bierman, P. R., Mickelson, D. M., & Caffee, M. (2002). Variation in glacial erosion near the southern margin of the Laurentide Ice Sheet, south-central Wisconsin, USA: Implications for cosmogenic dating of glacial terrains. *GSA Bulletin | GeoScienceWorld*. https://doi.org/10.1130/0016-7606(2002)114

Corbett, L. B., Bierman, P. R. and Davis, P.T. (2016) Glacial history and landscape evolution of southern Cumberland Peninsula, Baffin Island, Canada, constrained by cosmogenic ^{10}Be and ^{26}Al. Geological Society of America Bulletin. v. 128(7-8), p. 1173-1192. doi.org/10.1130/B31402.1

Corbett, L. B., Bierman, P. R., Neumann, T., Graly, J. A., Shakun, J. D., Goehring, B. M., Hidy, A. J., & Caffee, M. W. (2021). Measuring multiple cosmogenic nuclides in glacial cobbles sheds light on Greenland Ice Sheet processes. *Earth and Planetary Science Letters*, *554*, 116673. https://doi.org/10.1016/j.epsl.2020.116673

Corbett, L. B., Bierman, P. R., & Rood, D. H. (2016a). An approach for optimizing in situ cosmogenic ^{10}Be sample preparation. *Quaternary Geochronology*, *33*, 24–34. https://doi.org/10.1016/j.quageo.2016.02.001

Corbett, L. B., Bierman, P. R. and Rood, D. H. (2016b) Constraining multi-stage exposure-burial scenarios for boulders preserved beneath cold-based glacial ice in Thule, Northwest Greenland. *Earth and Planetary Science Letters*, *440*, 147–157. doi.org/10.1016/j.epsl.2016.02.004

Corbett, L. B., Bierman, P. R., Rood, D. H., Caffee, M. W., Lifton, N. A. and Woodruff, T. E. (2017), Cosmogenic ^{26}Al/^{10}Be surface production ratio in Greenland. *Geophysical Research Letters*, *44*(3), 1350-1359. doi.org/10.1002/2016GL071276

Couette, P., Ghienne, J., Lajeunesse, P., & Woerd, J. (2023). Climatic control on the retreat of the Laurentide Ice Sheet margin in easternmost Québec–Labrador (Canada) revealed by cosmogenic nuclide exposure dating. *Journal of Quaternary Science, 38*(7), 1044-1061. https://doi.org/10.1002/jqs.3525

Dalton, A., Finkelstein, S. A., Forman, S. L., Barnett, P. J., Pico, T., & Mitrovica, J. X. (2019). Was the Laurentide Ice Sheet significantly reduced during Marine Isotope Stage 3? *Geology*, *47*(2), 111–114. https://doi.org/10.1130/g45335.1

Dalton, A., Margold, M., Stokes, C., Tarasov, L., Dyke, A. S., Adams, R. S., Allard, S., Atends, H. E., Atkinson, N., Attig, J. W., Barnett, P., Barnett, R., Batterson, M., Bernatchez, P., Borns, H. W., Breckenridge, A., Briner, J. P., Brouard, E., Campbell, J. E., Carlson, A. E., Wright, H. E. (2020). An Updated Radiocarbon-Based Ice Margin Chronology for the Last Deglaciation of the North American Ice Sheet Complex. *Quaternary Science Reviews, 234*(15), 0277-3791. https://doi.org/10.1016/j.quascirev.2020.106223

Davis, P. T., Bierman, P. R., Marsella, K. A., Caffee, M. W., & Southon, J. (1999). Cosmogenic analysis of glacial terrains in the eastern Canadian Arctic: a test for inherited nuclides and the effectiveness of glacial erosion. *Annals of Glaciology*, *28*, 181–188. https://doi.org/10.3189/172756499781821805

Dethier, D. P., Racela, J., & Wieman, S. T. (2018). A contemporary mass-balance approach to small-catchment denudation rates in glaciated New England. *Abstracts With Programs - Geological Society of America*. https://doi.org/10.1130/abs/2018am-319718

Dunai, T. J., & Lifton, N. A. (2014). The nuts and bolts of cosmogenic nuclide production. *Elements*, *10*(5), 347–350. https://doi.org/10.2113/gselements.10.5.347

Dyke, A. S. (2004). An outline of North American deglaciation with emphasis on central and northern Canada. In *Developments in quaternary science* (pp. 373–424). https://doi.org/10.1016/s1571-0866(04)80209-4

Goehring, B. M., Kelly, M. A., Schaefer, J. M., Finkel, R. C., & Lowell, T. V. (2010). Dating of raised marine and lacustrine deposits in east Greenland using beryllium-10 depth profiles and implications for estimates of subglacial erosion. *JQS. Journal of Quaternary Science/Journal of Quaternary Science*, *25*(6), 865–874. https://doi.org/10.1002/jqs.1380

Gosse, J. C., & Phillips, F. M. (2001). Terrestrial in situ cosmogenic nuclides: theory and application. *Quaternary Science Reviews*, *20*(14), 1475–1560. https://doi.org/10.1016/s0277-3791(00)00171-2

Gregoire, L., Ivanović, R., Maycock, A. C., Valdes, P. J., & Stevenson, S. (2018). Holocene lowering of the Laurentide ice sheet affects North Atlantic gyre circulation and climate. *Climate Dynamics*, *51*(9–10), 3797–3813. https://doi.org/10.1007/s00382-018-4111-9

Halsted, C. T., Bierman, P. R., Shakun, J. D., Davis, P. T., Corbett, L. B., Drebber, J. S., & Ridge,

https://doi.org/10.5194/egusphere-2024-2233
Preprint. Discussion started: 29 July 2024
© Author(s) 2024. CC BY 4.0 License.

J. C. (2023). A critical re-analysis of constraints on the timing and rate of Laurentide Ice Sheet recession in the northeastern United States. *JQS. Journal of Quaternary Science/Journal of Quaternary Science*, *39*(1), 54–69. https://doi.org/10.1002/jqs.3563

Harbor, J. M., Stroeven, A. P., Fabel, D., Clarhäll, A., Klemån, J., Li, Y., Elmore, D., & Fink, D. (2006). Cosmogenic nuclide evidence for minimal erosion across two subglacial sliding boundaries of the late glacial Fennoscandian ice sheet. *Geomorphology*, *75*(1–2), 90–99. https://doi.org/10.1016/j.geomorph.2004.09.036

Hippe, K. (2017). Constraining processes of landscape change with combined in situ cosmogenic ^{14}C-^{10}Be analysis. *Quaternary Science Reviews*, *173*, 1–19. https://doi.org/10.1016/j.quascirev.2017.07.020

Hynes, A., & Rivers, T. (2010). Protracted continental collision — evidence from the Grenville Orogen. This article is one of a series of papers published in this Special Issue on the theme Lithoprobe — parameters, processes, and the evolution of a continent. *Canadian Journal of Earth Sciences*, *47*(5), 591–620. https://doi.org/10.1139/e10-003

Klein, J., Giegengack, R., Middleton, R., & Weeks, R. (1986). Revealing histories of exposure using insitu produced AL-26 and BE-10 in Libyan desert glass. *Radiocarbon*, *28*(547-555).

Kleman, J., Borgstrom, I., & Hattestrand, C. (1994). Evidence for a relict glacial landscape in Quebec-Labrador. Palaeogeography, Palaeoclimatology, Palaeoecology, 111(1994), 217-228.

Klemån, J., Jansson, K. N., De Angelis, H., Stroeven, A. P., Hättestrand, C., Alm, G., & Glasser, N. F. (2010). North American Ice Sheet build-up during the last glacial cycle, 115–21 kyr. *Quaternary Science Reviews*, *29*(17–18), 2036–2051. https://doi.org/10.1016/j.quascirev.2010.04.021

LeBlanc, D. E., Shakun, J. D., Corbett, L. B., Bierman, P. R., Caffe, M. W., & Hidy, A. J. (2023). Laurentide Ice Sheet Persistence During Pleistocene Interglacials. *Geology, 51*(5), 496-499. https://doi.org/10.1130/G50820.1

Larsen, H. C., Saunders, A. D., Clift, P. D., Beget, J., Wei, W., and Spezzaferri, S.: Seven million years of glaciation in Greenland, Science, 264, 952–955, https://doi.org/10.1126/science.264.5161.952, 1994.

Larue, F., Royer, A., De Sève, D., Langlois, A., Roy, A., & Brucker, L. (2017). Validation of GlobSnow-2 snow water equivalent over Eastern Canada. *Remote Sensing of Environment*, *194*, 264–277. https://doi.org/10.1016/j.rse.2017.03.027

Margold, M., Stokes, C. R., & Clark, C. D. (2015). Ice streams in the Laurentide Ice Sheet: Identification, characteristics and comparison to modern ice sheets. *Earth-science Reviews*, *143*, 117–146. https://doi.org/10.1016/j.earscirev.2015.01.011

Margold, M., Stokes, C. R., & Clark, C. D. (2018). Reconciling records of ice streaming and ice margin retreat to produce a palaeogeographic reconstruction of the deglaciation of the Laurentide Ice Sheet. *Quaternary Science Reviews*, *189*, 1–30. https://doi.org/10.1016/j.quascirev.2018.03.013

Marsella, K. A., Bierman, P. R., Davis, P. T. and Caffee, M. W. (2000) Cosmogenic ^{10}Be and ^{26}Al ages for the last glacial maximum, eastern Baffin Island, Arctic Canada. *Geological Society of America Bulletin*. v. 112(8), p. 1296-1312. doi.org/10.1130/0016-7606(2000)112<1296:CBAAAF>2.0.CO;2

Marshall, S. J., Tarasov, L., Clarke, G. K. C., & Peltier, W. R. (2000). Glaciological reconstruction of the Laurentide Ice Sheet: physical processes and modelling challenges. *Canadian Journal of Earth Sciences*, *37*(5), 769–793. https://doi.org/10.1139/e99-113

Melanson, A., Bell, T., & Tarasov, L. (2013). Numerical modelling of subglacial erosion and sediment transport and its application to the North American ice sheets over the Last Glacial cycle. *Quaternary Science Reviews*, *68*, 154–174. https://doi.org/10.1016/j.quascirev.2013.02.017

Miller, G. H., & Andrews, J. T. (2019). Hudson Bay was not deglaciated during MIS-3. *Quaternary Science Reviews*, *225*, 105944. https://doi.org/10.1016/j.quascirev.2019.105944

Munroe, J. S., Perzan, Z., & Amidon, W. H. (2016). Cave sediments constrain the latest Pleistocene advance of the Laurentide Ice Sheet in the Champlain Valley, Vermont, USA. *JQS. Journal of Quaternary Science/Journal of Quaternary Science*, *31*(8), 893–904. https://doi.org/10.1002/jqs.2913

Nelson, A. H., Bierman, P. R., Shakun, J. D., & Hood, D. H. (2014). Using in situ cosmogenic ^{10}Be to identify the source of sediment leaving Greenland. *Earth Surface Processes and Landforms, 39*, 1087-1100. 10.1002/esp.3565

Nishiizumi, K. (2004). Preparation of ^{26}Al AMS standards. *Nuclear Instruments and Methods in Physics Research. Section B, Beam Interactions with Materials and Atoms/Nuclear Instruments & Methods in Physics Research. Section B, Beam Interactions with Materials and Atoms*, *223–224*, 388–392. https://doi.org/10.1016/j.nimb.2004.04.075

https://doi.org/10.5194/egusphere-2024-2233
Preprint. Discussion started: 29 July 2024
© Author(s) 2024. CC BY 4.0 License.

Nishiizumi, K., Kohl, C. P., Arnold, J. R., Klein, J., Fink, D., & Middleton, R. (1991). Cosmic ray produced ^{10}Be and ^{26}Al in Antarctic rocks: exposure and erosion history. *Earth and Planetary Science Letters*, *104*(2–4), 440–454. https://doi.org/10.1016/0012-821x(91)90221-3

Nishiizumi, K., Imamura, M., Caffee, M. W., Southon, J., Finkel, R. C., & McAninch, J. (2007). Absolute calibration of ^{10}Be AMS standards. *Nuclear Instruments and Methods in Physics Research. Section B, Beam Interactions with Materials and Atoms/Nuclear Instruments & Methods in Physics Research. Section B, Beam Interactions with Materials and Atoms*, *258*(2), 403–413. https://doi.org/10.1016/j.nimb.2007.01.297

Nishiizumi, K., Winterer, E. L., Kohl, C. P., Klein, J., Middleton, R., Lal, D., & Arnold, J. R. (1989). Cosmic ray production rates of ^{10}Be and ^{26}Al in Antarctic rocks: exposure and erosion history in quartz from glacially polished rocks. *Earth and Planetary Science Letters*, *104Journal of Geophysical Research*, *94*(B12), 17907–17915. https://doi.org/10.1029/jb094ib12p17907

Payette, S., Morneau, C., Sirois, L., & Desponts, M. (1989). Recent fire history of the Northern Quebec Biomes. *Ecology*, *70*(3), 656–673. https://doi.org/10.2307/1940217

Pico, T., Birch, L., Weisenberg, J., & Mitrovica, J. (2018). Refining the Laurentide Ice Sheet at Marine Isotope Stage 3: A data-based approach combining glacial isostatic simulations with a dynamic ice model. *Quaternary Science Reviews*, *195*, 171–179. https://doi.org/10.1016/j.quascirev.2018.07.023

Rasmussen, S. O., Andersen, K. H., Svensson, A., Steffensen, J. P., Vinther, B. M., Clausen, H., Siggaard-Andersen, M., Johnsen, S. J., Larsen, L. H., Dahl-Jensen, D., Bigler, M., Röthlisberger, R., Fischer, H., Goto-Azuma, K., Hansson, M., & Ruth, U. (2006). A new Greenland ice core chronology for the last glacial termination. *Journal of Geophysical Research*, *111*(D6). https://doi.org/10.1029/2005jd006079

Rice, J., Ross, M., Paulen, R., Kelley, S., & Briner, J. (2020). A GIS-based multi-proxy analysis of the evolution of subglacial dynamics of the Quebec–Labrador ice dome, northeastern Quebec, Canada. *Earth Surface Processes and Landforms*, *45*(13), 3155–3177. https://doi.org/10.1002/esp.4957

Rice, J. M., Ross, M., Paulen, R. C., Kelley, S. E., Briner, J. P., Neudorf, C. M., & Lian, O. B. (2019). Refining the ice flow chronology and subglacial dynamics across the migrating Labrador Divide of the Laurentide Ice Sheet with age constraints on deglaciation. *JQS. Journal of Quaternary Science/Journal of Quaternary Science*, *34*(7), 519–535. https://doi.org/10.1002/jqs.3138

Rivers of Canada - Churchill River : Can Geo Education. (n.d.). https://web.archive.org/web/20200201124628/http://www.cangeoeducation.ca/resources/rivers_of_canada/churchill_river/default.asp

Roy, M., Hemming, S. R., & Parent, M. (2009). Sediment sources of northern Québec and Labrador glacial deposits and the northeastern sector of the Laurentide Ice Sheet during ice-rafting events of the last glacial cycle. *Quaternary Science Reviews*, *28*(27–28), 3236–3245. https://doi.org/10.1016/j.quascirev.2009.08.008

Spray, J. G., Kelley, S. P., & Rowley, D. B. (1998). Evidence for a late Triassic multiple impact event on Earth. *Nature*, *392*(6672), 171–173. https://doi.org/10.1038/32397

Staiger, J. K. W., Gosse, J. C., Johnson, J. V., Fastook, J. L., Gray, J., Stöckli, D. F., Stockli, L. D., & Finkel, R. C. (2005). Quaternary relief generation by polythermal glacier ice. *Earth Surface Processes and Landforms*, *30*(9), 1145–1159. https://doi.org/10.1002/esp.1267

Staiger, J. W., Marchant, D. R., Schaefer, J. M., Oberholzer, P., Johnson, J. V., Lewis, A. R., & Swanger, K. M. (2006). Plio-Pleistocene history of Ferrar Glacier, Antarctica: Implications for climate and ice sheet stability. *Earth and Planetary Science Letters*, *243*(3–4), 489–503. https://doi.org/10.1016/j.epsl.2006.01.037

Stokes, C. R., Tarasov, L., Blomdin, R., Cronin, T. M., Fisher, T. G., Gyllencreutz, R., Hättestrand, C., Heyman, J., Hindmarsh, R. C., Hughes, A. L., Jakobsson, M., Kirchner, N., Livingstone, S. J., Margold, M., Murton, J. B., Noormets, R., Peltier, W. R., Peteet, D. M., Piper, D. J., . . . Teller, J. T. (2015). On the reconstruction of palaeo-ice sheets: Recent advances and future challenges. *Quaternary Science Reviews*, *125*, 15–49. https://doi.org/10.1016/j.quascirev.2015.07.016

Stokes, C. R., Tarasov, L., & Dyke, A. S. (2012). Dynamics of the North American Ice Sheet Complex during its inception and build-up to the Last Glacial Maximum. *Quaternary Science Reviews*, *50*, 86–104. https://doi.org/10.1016/j.quascirev.2012.07.009

Storrar, R. D., Stokes, C. R., & Evans, D. J. (2013). A map of large Canadian eskers from Landsat satellite imagery. *Journal of Maps*, *9*(3), 456–473. https://doi.org/10.1080/17445647.2013.815591

https://doi.org/10.5194/egusphere-2024-2233
Preprint. Discussion started: 29 July 2024
© Author(s) 2024. CC BY 4.0 License.

Stroeven, A. P., Fabel, D., Hättestrand, C., & Harbor, J. M. (2002). A relict landscape in the centre of Fennoscandian glaciation: cosmogenic radionuclide evidence of tors preserved through multiple glacial cycles. *Geomorphology*, *44*(1–2), 145–154. https://doi.org/10.1016/s0169-555x(01)00150-7

Süfke, F., Gutjahr, M., Keigwin, L. D., Reilly, B. T., Giosan, L., & Lippold, J. (2022). Arctic drainage of Laurentide Ice Sheet meltwater throughout the past 14,700 years. *Communications Earth & Environment*, *3*(1). https://doi.org/10.1038/s43247-022-00428-3

Tarasov, L., Dyke, A. S., Neal, R. M., & Peltier, W. R. (2012). A data-calibrated distribution of deglacial chronologies for the North American ice complex from glaciological modeling. *Earth and Planetary Science Letters*, *315–316*, 30–40. https://doi.org/10.1016/j.epsl.2011.09.010

Ullman, D. (2023). The retreat chronology of the Laurentide Ice Sheet during the last 10,000 years and implications for deglacial sea-level rise. *Vignettes:Key Concepts in Geomorphology*. https://serc.carleton.edu/59463.

Ullman, D., Carlson, A. E., Hostetler, S. W., Clark, P. U., Cuzzone, J., Milne, G. A., Windsor, K., & Caffe, M. (2016). Final Laurentide ice-sheet deglaciation and Holocene climate-sea level change. *Quaternary Science Reviews, 152*(15), 49.59. https://doi.org/10.1016/j.quascirev.2016.09.014